MCR RapidIMPACT

Molecular Cancer Research

A Human Genome-Wide RNAi Screen Reveals Diverse Modulators that Mediate IRE1α–XBP1 Activation

Zhifen Yang[1], Jing Zhang[1], Dadi Jiang[2], Purvesh Khatri[3], David E. Solow-Cordero[4], Diego A.S. Toesca[1], Constantinos Koumenis[5], Nicholas C. Denko[6], Amato J. Giaccia[1], Quynh-Thu Le[1], and Albert C. Koong[2]

Abstract

Activation of the unfolded protein response (UPR) signaling pathways is linked to multiple human diseases, including cancer. The inositol-requiring kinase 1α (IRE1α)–X-box binding protein 1 (XBP1) pathway is the most evolutionarily conserved of the three major signaling branches of the UPR. Here, we performed a genome-wide siRNA screen to obtain a systematic assessment of genes integrated in the IRE1α–XBP1 axis. We monitored the expression of an XBP1-luciferase chimeric protein in which luciferase was fused in-frame with the spliced (active) form of XBP1. Using cells expressing this reporter construct, we identified 162 genes for which siRNA inhibition resulted in alteration in XBP1 splicing. These genes express diverse types of proteins modulating a wide range of cellular processes. Pathway analysis identified a set of genes implicated in the pathogenesis of breast cancer. Several genes, including *BCL10*, *GCLM*, and *IGF1R*, correlated with worse relapse-free survival (RFS) in an analysis of patients with triple-negative breast cancer (TNBC). However, in this cohort of 1,908 patients, only high GCLM expression correlated with worse RFS in both TNBC and non-TNBC patients. Altogether, our study revealed unidentified roles of novel pathways regulating the UPR, and these findings may serve as a paradigm for exploring novel therapeutic opportunities based on modulating the UPR.

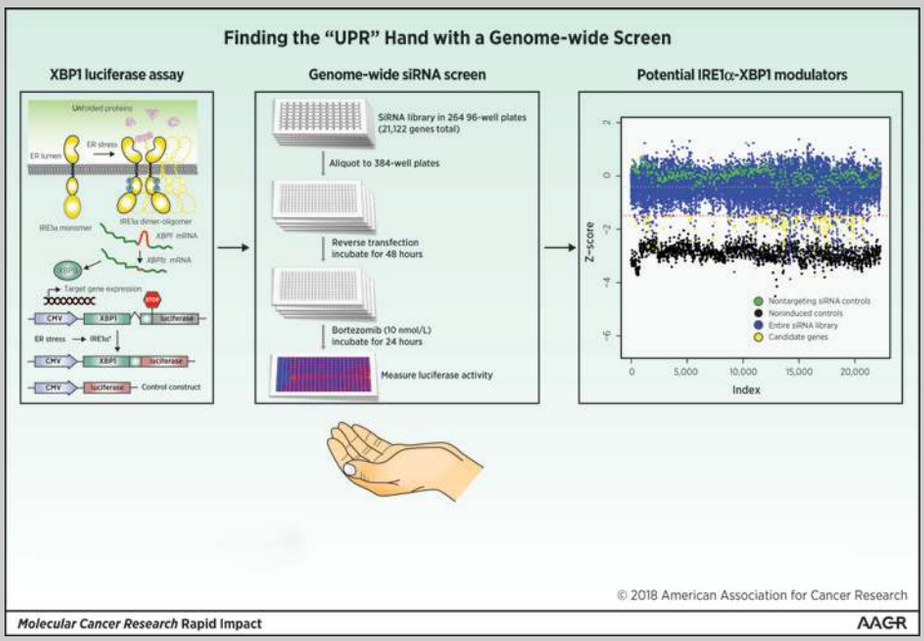

Implications: Genome-wide RNAi screen identifies novel genes/pathways that modulate IRE1α–XBP1 signaling in human tumor cells and leads to the development of improved therapeutic approaches targeting the UPR.

Visual Overview: http://mcr.aacrjournals.org/content/molcanres/16/5/745/F1.large.jpg. *Mol Cancer Res; 16(5); 745–53. ©2018 AACR.*

[1]Department of Radiation Oncology, Stanford University, Stanford, California. [2]Department of Radiation Oncology, The University of Texas MD Anderson Cancer Center, Houston, Texas. [3]Institute for Immunity, Transplantation and Infection, and Biomedical Informatics Research, Department of Medicine, Stanford University, Stanford, California. [4]High-Throughput Bioscience Center, Department of Chemical and Systems Biology, Stanford University, Stanford, California. [5]Department of Radiation Oncology, University of Pennsylvania School of Medicine, Philadelphia, Pennsylvania. [6]Department of Radiation Oncology, The Ohio State University, Columbus, Ohio.

Note: Supplementary data for this article are available at Molecular Cancer Research Online (http://mcr.aacrjournals.org/).

Z. Yang and J. Zhang contributed equally to this article.

Correspondence Author: Albert C. Koong, Department of Radiation Oncology, The University of Texas MD Anderson Cancer Center, 1515 Holcombe Blvd, Unit 1422, Houston, TX 77030. Phone: 713-563-2300; E-mail: akoong@mdanderson.org

doi: 10.1158/1541-7786.MCR-17-0307

Introduction

The endoplasmic reticulum (ER) is the central organelle responsible for protein synthesis, assembly, and secretion. Perturbation of these processes by stresses in the tissue microenvironment, including glucose deprivation, hypoxia, and chemotherapeutic agents, leads to the accumulation of misfolded or unfolded proteins in the ER lumen, causing ER stress (1). To restore cellular homeostasis, cells have developed an evolutionarily conserved signaling network known as the unfolded protein response (UPR). In the presence of ER stress, the UPR is induced to promote cell survival by reducing protein translation, increasing the expression of ER chaperones and protein folding enzymes, and targeting misfolded proteins for degradation (1). However, under conditions of prolonged ER stress, the UPR may also activate proapoptotic signaling (2).

Three ER-resident transmembrane proteins are responsible for sensing ER stress and triggering UPR signaling: inositol-requiring kinase 1α (IRE1α), double-stranded RNA-activated protein kinase (PKR)–like endoplasmic reticulum kinase (PERK), and activating transcription factor 6 (ATF6; ref. 1). IRE1α is a type I transmembrane protein that has two catalytic domains, a serine/threonine kinase domain and an endoribonuclease domain at the carboxyl terminal. In the presence of ER stress, IRE1α dimerizes and oligomerizes, then autophosphorylates through its kinase domain, leading to the activation of the endoribonuclease domain (3, 4). The activated endoribonuclease domain excises a 26-nucleotide intron from the mRNA encoding a basic leucine zipper (bZIP) transcription factor, X-box–binding protein 1 (XBP1). The removal of the 26-nucleotide sequence causes a translational frame shift and results in the production of a larger, spliced form of XBP1 protein (XBP1s), which is a potent transcriptional activator of various UPR-targeted genes (Fig. 1A; refs. 1, 5).

The IRE1α–XBP1 pathway plays an important role in various human diseases (5). XBP1 is a key regulator of glucose intolerance and insulin resistance in diabetes (6). In cancer, several lines of evidence demonstrate a critical role for the IRE1α–XBP1 pathway in tumor growth, metastasis, and immune function (7, 8). Tumor growth and survival under hypoxic conditions were severely compromised when XBP1 expression was inhibited (9). As a mediator of cell survival, XBP1 activation has been extensively characterized in multiple myeloma, a plasma cell malignancy (10, 11). XBP1 is essential for plasma cell differentiation, and its expression is elevated in human multiple myeloma cells, and XBP1s expression is associated with poor multiple myeloma patient survival (12, 13). Consistent with these observations, expression and activation of XBP1 have also been correlated with poor clinical outcome in breast cancer, and with angiogenesis in pancreatic cancer (14–16). In breast cancer cells, knockdown of XBP1 expression inhibited tumor growth and relapse (15). Small-molecule inhibitors that selectively block IRE1α endoribonuclease activity and XBP1s expression have displayed potent antitumor activity in multiple cancer types (5, 7, 17–20).

Accumulating evidence indicates that the UPR signaling integrates information regarding the intensity and the duration of the stress stimuli to generate signaling leading to prosurvival or proapoptotic pathways (5). However, mechanistic understanding of these pathways, particularly their relevance to human disease, is incomplete (5, 8). More importantly, current knowledge regarding the regulation of XBP1 activity in cancer remains elusive despite its reported functional significance in these diseases (5, 21). Therefore, to extend our understanding of the molecular basis of the UPR, we conducted an siRNA screen as a strategy to identify novel genes/pathways that modulate IRE1α–XBP1 signaling in human tumor cells. Ultimately, this knowledge will lead to the development of improved therapeutic approaches targeting the UPR.

Materials and Methods

Cell culture

Human fibrosarcoma HT1080 and human breast cancer MCF7 and MDA-MB-231 cells were originally purchased from the ATCC and immediately expanded and frozen down as master stocks. Cells were passaged for 3 months and then replaced with fresh stocks. Authentication of these cell lines was performed by short tandem repeat profiling at the Stanford Functional Genomics Facility. Cells were routinely monitored for mycoplasma contamination by the MycoAlert Mycoplasma Detection Kit (Lonza). Cells were maintained at 37°C with 5% CO_2 in DMEM media (Gibco) supplemented with 100 U/mL penicillin/streptomycin antibiotics and 10% FBS. HT1080 cells stably expressing the XBP1-luc or CMV-luc constructs were established as described previously (22, 23). We also used mouse embryonic fibroblasts (MEF) expressing the human IGF1 receptor (R^+) and *IGF1R* knockout (R^-) MEF cells obtained courtesy of Renato Baserga (Thomas Jefferson University, Philadelphia, PA; ref. 24).

CRISPR/Cas9–mediated knockout of *BCL10* or *GCLM*

BCL10- or *GCLM*-knockout MCF7 or MDA-MB-231 cell lines were established by CRISPR/Cas9–mediated genome editing. Guide RNA sequences (sgRNA) for CRISPR/Cas9 were designed using http://crispr.mit.edu/ hosted by the Feng Zhang Lab. Oligonucleotide inserts for generating human *BCL10* and *GCLM* gRNAs are the following: 5′-CTCGCCGAATAGATTCAACA-3′ (*BCL10*, Exon 2) and 5′-GTGCCCGTCCACGCACAGCG-3′ (*GCLM*, Exon 1). The complementary oligonucleotides for the gRNAs were annealed and cloned into the lentiCRISPR v2 vector (Addgene, plasmid #52961; ref. 25). Lentiviral particles were produced by cotransfection with psPAX2 and pMD2.G plasmids into HEK293T cells. Viral supernatants were collected 48 to 60 hours posttransfection and cleared through a 0.45-μm filter and used to infect human breast cancer cells (MCF7 and MDA-MB-231) for three rounds with Polybrene supplement (4 μg/mL; Sigma). After final infection, stable populations were obtained by selection with 2 μg/mL puromycin (Invitrogen). After 2 weeks, colonies were isolated and screened for BCL10 or GCLM expression by Western blotting.

siRNA transfection and siRNA screen

For the primary screen, we used an arrayed library of 21,121 siRNA pools covering the majority of the human genome [Dharmacon Human Genome siARRAY siRNA library (cat# G-005000-025), Thermo Fisher Scientific]. Each siRNA pool consisted of four oligonucleotides targeting different regions of the same gene. Each assay plate included the following controls: nontargeting control siRNA, siTOX control siRNA, and *ERN1* (human IRE1α) siRNA (Thermo Fisher Scientific). The siRNAs were transiently transfected in duplicate into HT1080 cells stably expressing the XBP1-luc or CMV-luc reporter at a 25 nmol/L final concentration using reverse transfection. In detail, all siRNAs were

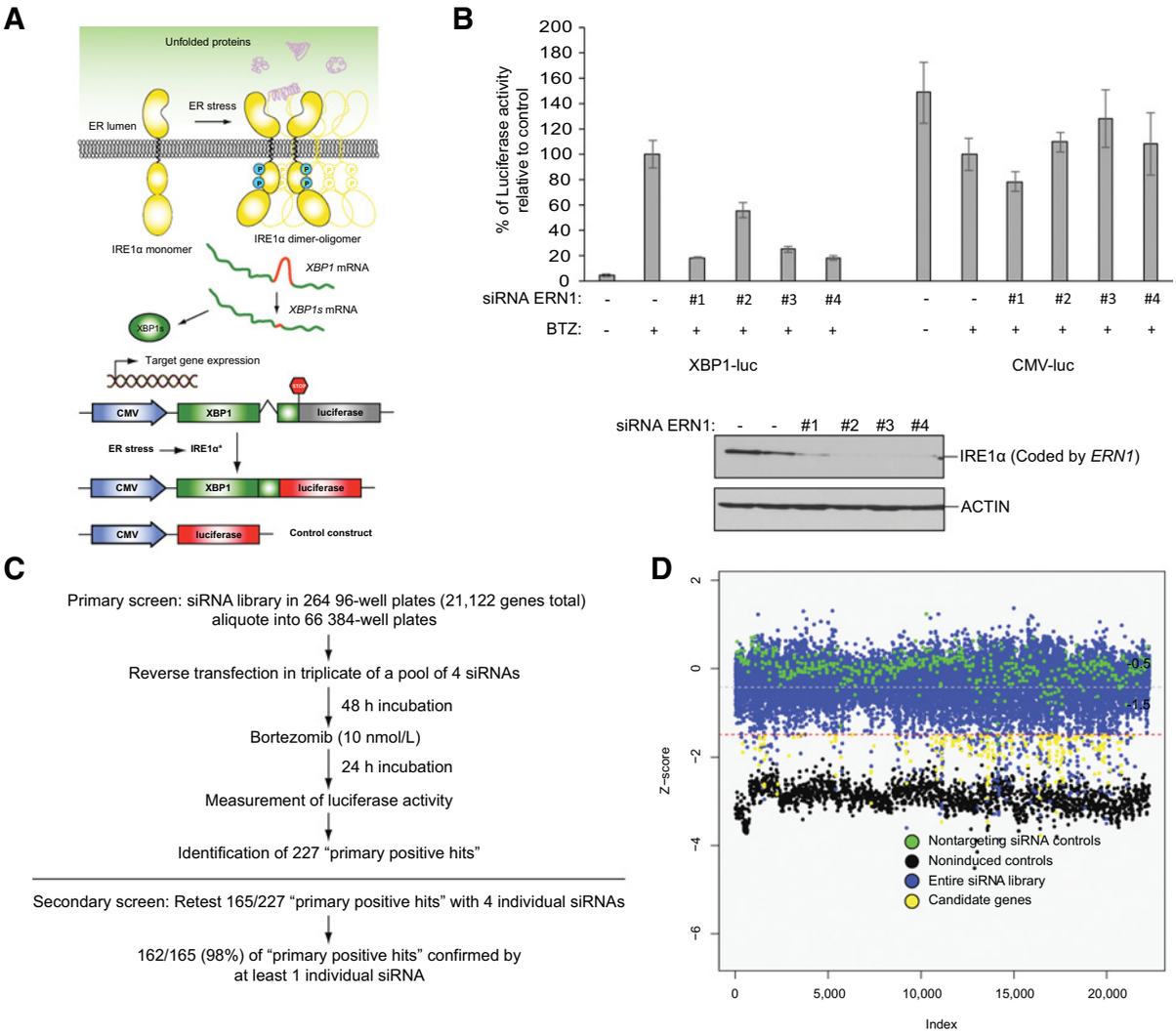

Figure 1.

Whole-genome siRNA screen for genes required for optimal XBP1 splicing. **A,** Top, schematic overview of ER stress-induced IRE1α activation and *XBP1* mRNA splicing; bottom, schematic view of the luciferase reporter constructs used in this study. **B,** HT1080-XBP1-luc and HT1080-CMV-luc cells were transfected with nontargeting siRNA (control) or siRNA targeting human *ERN1* for 48 hours, and then treated with bortezomib (BTZ, 10 nmol/L) for 24 hours, and luciferase activity was measured. **C,** Summary of the siRNA screen approach. **D,** Dot plot of the screen results. *y*-axis represents the average *z*-scores of HT1080-XBP1-luc luminescence readings for each targeted gene. Nontargeting siRNA controls are colored in green. Noninduced controls are colored in black. The entire siRNA library is colored in blue with candidate genes highlighted in yellow. Red dash line represents cut-off *z*-score of −1.5. Gray dash line represents cutoff *z*-score of −0.5.

aliquoted into 384-well plates (8 μL/well) in duplicate for each cell line using an Agilent Technologies (formerly Velocity 11) robotic system. To each well, 10 μL of serum-free DMEM media containing 0.04 μL Dharmafect 1 transfection reagent (Dharmacon) was added using WellMate Dispenser (Matrix). The siRNA/Dharmafect mixture was incubated at room temperature for 1 hour before 60 μL of HT1080-XBP1-luc or HT1080-CMV-luc cell suspension (10,000 cells/mL in complete DMEM media) was seeded using the WellMate Dispensing system. After incubation at room temperature for 30 minutes, all plates were placed into cell culture incubator at 37°C supplied with 5% CO_2. ER stress was induced by adding 10 μL of bortezomib (10 nmol/L) after 48 hours to all the wells except the first two columns of each plate, which served as a noninduced control. The plates were returned to the incubator for additional 24 hours before the luciferase assay was performed.

For the secondary screen, the 4 oligonucleotides of each siRNA pool were added into individual wells. The cells were transfected and treated with bortezomib using the same procedure as for the primary screen.

In the validation studies, HT1080 cells were transfected in 6-well or 6-cm plates using reverse transfection with 1.25 μL Dharmafect 1/mL, 10 to 20 nmol/L final siRNA concentration, and cells at 1×10^5 to 2.5×10^5 cells/mL. After incubation for 48 hours at 37 °C, ER stress was induced by thapsigargin or bortezomib treatment at 300 or 100 nmol/L final concentration, respectively. Cells were harvested after 14 hours under ER stress and further assessed by Western blotting or qRT-PCR.

Luciferase reporter assay

To measure the luciferase activity in both HT1080-XBP1-luc and HT1080-CMV-luc cells, we performed luciferase reporter assay. For siRNA screen in 384-well plates, 10 μL per well of Bright-Glo firefly luciferase substrate (Promega) was added, and luciferase activity was measured immediately using Analyst GT plate reader (Molecular Devices) in coordination with Twister II robotic loading system (Caliper LS). For luciferase assays in 96-well plates, 20 μL per well of Bright-Glo substrate was added before the plates were read using Tecan Infinite M1000 multimode plate reader (Tecan Group).

Statistical analysis

To effectively identify initial hits and minimize false positives, we included several quality controls and performed step-by-step statistical analysis. The controls were the following: (i) blank: transfection reagents only and were treated with DMSO control; (ii) low control: siTOX control siRNA plus transfection reagents and were treated with bortezomib; (iii) high control: nontargeting control siRNA plus transfection reagents and were treated bortezomib; (iv) negative control: transfection reagents only and were treated with bortezomib; (v) positive control: human *ERN1* siRNA plus transfection reagents and were treated with bortezomib.

All the luminescence readout data were first transformed to logarithmic scale. Then, each plate was normalized using a median of positive control wells on a given plate for intraplate normalization. We performed interplate normalization by computing median of luminescence intensity value across all plates and then scaling each plate to have the same median value. Using the normalized luminescence, we computed *z*-score such that a negative *z*-score indicated inhibition of XBP1-luciferase and a positive *z*-score indicated activation of XBP1-luciferase. The screen hits were selected on the basis of the median *z*-score of the duplicate plates with a cut-off of *z*-score <-1.5. We chose a *z*-score cutoff of -1.5 to efficiently reduce false negatives. The resulting hits were subjected to a more stringent secondary screen to rule out false positive hits.

To analyze the secondary screen data, the normalized percentage of inhibition for each siRNA compared with nontargeting control was calculated. We used percentage of inhibition as follows: % of inhibition $= [1-[(\text{response}-\text{low})/(\text{high}-\text{low})]] * 100$; response = the raw data for each well (luminescence signal); low = median of low control, siTOX wells; high = median of high control, siGenome nontargeting wells. We used 50% normalized inhibition as a threshold. An siRNA that inhibits XBP1-luciferase signal no less than 50% was selected. To exclude siRNAs that have general toxic effect, we applied a 50% normalized percentage of inhibition to the CMV-luciferase cell line. An siRNA that inhibits CMV-luciferase activity by more than 50% was considered toxic and thus eliminated from further analysis. The remaining siRNAs were considered to inhibit XBP1 splicing significantly and specifically.

Unless otherwise indicated, all the *P* values in this study were calculated from a two-tailed Student *t* test with equal variance. All error bars represent standard deviation.

Bioinformatic analysis

Reactome Skypainter (www.reactome.org/skypainter-2/) and Ingenuity Pathway Analysis (IPA, www.ingenuity.com/products/ipa) for pathway analysis were used to select genes for our secondary screen. Using a list of input genes, Reactome Skypainter identifies which pathways these genes are involved in and computes *P* values for observing that many or more genes in a given pathway. Because Skypainter does not correct these *P* values for multiple hypotheses, Benjamini–Hochberg correction was applied to identify pathways with significance at FDR $\leq$ 5%. The list of initial 227 genes was used as input of IPA for network analysis. When creating the gene–gene interaction networks, the "direct relationships" option in IPA analysis was implemented.

Western blotting

Cells were lysed in RIPA buffer (Cell Signaling Technology) and protein concentration was determined using the Bradford protein assay (Bio-Rad). Lysates (50 μg) were separated using 10% SDS-PAGE and electro-transferred onto Nitrocellulous membranes (Bio-Rad) following standard protocols. Antibodies used include anti-XBP1s (BioLegend), anti-BCL10, anti-GCLM and anti-β actin (Santa Cruz Biotechnology), and anti-IGF1R (Cell Signaling Technology). Chemiluminescence was induced with ECL detection reagents (GE Healthcare) and measured using ChemiDoc system (Bio-Rad). Blots were quantified using NIH ImageJ64 software.

Analysis of breast cancer patient datasets

Microarray expression and clinical data of the 1,809 patients were downloaded from Kaplan–Meier Plotter website (www.kmplot.com). The estrogen receptor (ESR) and the triple-negative breast cancer (TNBC) status of each patient tumor sample in this dataset was defined as reported previously (26, 27). The Kaplan–Meier relapse-free survival (RFS) graphs of the different subtypes of patients with breast cancer stratified by the expression of BCL10, GCLM, or IGF1R were plotted as described previously (28). The RNA-seq data ($n = 1{,}182$; Illumina HiSeq) with the clinical information of the patients with breast cancer were downloaded from The Cancer Genome Atlas (TCGA) database through the University of California Santa Cruz Cancer Browser. Correlations between the expression of BCL10, GCLM or IGF1R and XBP1 gene signature were evaluated using Pearson correlation matrix (28).

Results and Discussion

Genome-wide siRNA screen

To identify genes that are required for XBP1 activation under UPR, we performed a whole-genome high-throughput siRNA screen using a unique quantitative signal–monitoring system. In this system, the coding sequence of firefly luciferase is fused in-frame with the human XBP1s mRNA sequence, resulting in luciferase expression only when XBP1 mRNA is spliced into its active XBP1s form. This construct, or a CMV promoter-driven luciferase construct used to normalize for nonspecific effects, was stably introduced into HT1080 human fibrosarcoma cells (HT1080-XBP1-luc and HT1080-CMV-luc, respectively; Fig. 1A; ref. 29). ER stress was induced by the administration of 10 nmol/L bortezomib, and luciferase activity was measured after 24 hours. Bortezomib is a selective and potent inhibitor of the 26S proteasome, as well as a modulator of calcium flux within the ER (30). Treatment of cells with this agent induced the UPR (31) and XBP1 splicing (20). Transfection of siRNA targeting IRE1α (encoded by *ERN1*) led to significant inhibition of XBP1 splicing, as assessed by reduction of XBP1-luciferase activity,

but not CMV-luciferase activity (Fig. 1B). Using this system, we screened the siARRAY whole human genome siRNA library targeting 21,121 genes. The screening protocol is illustrated in Fig. 1C. The entire assay was carried out in duplicate for both cell lines, and normalized *z*-scores of luminescence were calculated. Our analyses focused on the group of screening hits in which siRNA inhibition of the gene resulted in differential inhibition of XBP1 splicing without reducing CMV-luciferase activity significantly. We selected genes with a *z*-score less than −1.5 to be considered significant for XBP1-luciferase inhibition (Fig. 1D). To reduce the false-positive hit rate, we used a more stringent *z*-score of less than −0.5 for CMV-luciferase activity as an indication of nonspecific activity (Fig. 1D; Supplementary Fig. S1A–S1D). Details of the statistical analysis are described in the Materials and Methods section.

Gene function and pathway analysis

The primary screen identified 227 candidate genes as potential regulators of IRE1α–XBP1 signaling (Supplementary Table S1). Gene Ontology analysis classified these genes into enzymes, transcriptional factors, transporters, phosphatases, peptidases, transmembrane receptors, and kinases (Fig. 2A). To identify genes that were significantly enriched in particular biological processes, we performed pathway enrichment analysis using Reactome Skypainter. The output demonstrates a global overview of significantly enriched pathways as illustrated in Fig. 2B. The most enriched genes include those encoding proteins involved in "mRNA Processing" and "Transcription" ($P < 10^{-5}$ and $P < 10^{-2}$, respectively; Fig. 2C). These findings were reassuring as transcription and mRNA processing are known to be involved in regulating XBP1 mRNA splicing during ER stress. Other significantly enriched signaling pathways include "Ion Channel Transport," "Gene Expression," "DNA Repair," and "Transmembrane Transport" (Fig. 2B and C), which are not previously associated with the UPR. The statistical significance of each enriched pathway is listed in Supplementary Table S2.

To examine whether these genes are part of specific signaling modules, we also created gene–gene interaction networks using IPA (Ingenuity Systems, Inc.). This analysis revealed two major interaction networks (Fig. 2D). Consistent with the Reactome Skypainter results, both networks contained a subset of genes involved in mRNA processing (Fig. 2D, orange dashed circle). Both networks also encompassed several genes that have been implicated in human cancers, including *BCL10*, *EPO*, *SMAD2*, and *CDKN1B* (*p27*) and are key regulators of cell cycle, proliferation, differentiation, and apoptosis. Particularly, we identified a subset of genes related to estrogen receptor signaling (Fig. 2D, blue dashed circle). Indeed, a majority of these genes, including *BCL10*, *GCLM*, *NCOR2* (*SMERT*), *CDKN1B* (*p27*), *HXOD1*, *IL-17A*, and *IGF1R*, have been shown to be critical for the onset and progression of breast cancer (32–37). It has been shown previously that XBP1 expression and activation correlated with clinical outcome of endocrine-treated breast cancer, resulting in tamoxifen resistance (14). Therefore, the interaction between these identified genes and XBP1 activation may play a significant role in the pathogenesis of human breast cancer.

Validation of the screen hits

Next, we chose a subset of 165 genes from the 227-gene list to confirm the reproducibility of the screen results using multiple individual siRNAs (deconvolution, Fig. 1C). The genes were selected based upon the Gene Ontology and functional analysis (as described in Materials and Methods and Supplementary Table S3). In this secondary screen, four siRNAs targeting different regions of the same gene were individually evaluated at 25 nmol/L with the same protocol used in the primary screen. To exclude siRNAs causing general cytotoxicity, we again included the HT1080-CMV-luc cells as a control. An siRNA was considered to be a positive hit if it inhibited XBP1-luciferase activity by more than 50% in comparison with the nontargeting control without significantly inhibiting the CMV-luciferase (below 50%). The details of the secondary screen are described in Materials and Methods. After applying these criteria, a total of 162 of the 165 candidate genes (98%) retested showed inhibition with at least 1 siRNA meeting the selection criteria. In addition, 56% of the genes (93/165), including *ERN1* (encoding IRE1α) and *XBP1*, had at least 3 of 4 siRNAs that met the selection criteria. The complete list of these genes and their secondary validation data are summarized in Supplementary Table S3. Seven (4.3%) of these genes, *XBP1*, *ERN1*, *GCLM*, *IGF1R*, *MCL-1*, *PIK3R5*, and *SEC61B* (21, 38–42), were previously identified to be related to IRE1α–XBP1 signaling. The identification of these known molecular connections provides an important validation of the screening approach we adopted.

To further substantiate our findings, we selected several screening hits representing each group (listed in Supplementary Table S3) for further validation. We performed qRT-PCR and/or Western blotting analysis of selected siRNA hits to determine the efficiency of gene knockdown (Supplementary Figs. S2A and S2B and S3A–S3D; and data not shown). XBP1 splicing was induced by either bortezomib or thapsigargin, an inhibitor of the ER Ca^{2+} ATPase to induce ER stress. siRNA knockdown of *BCL10*, *ERN1*, *GCLM*, *IGF1R*, *DAG1*, *FBXO4*, or *SERGEF* inhibited XBP1 splicing induced by either bortezomib or thapsigargin (Supplementary Fig. S2A and S2B). As summarized in Supplementary Table S4, of the 25 genes selected from the secondary screen, we identified 21 genes (88%) that were required for bortezomib-induced XBP1 splicing and 13 genes (52%) that were also essential for thapsigargin-induced XBP1 splicing (Supplementary Figs. S2A and S2B and S3A–S3D).

Recently, we and other investigators have shown that higher expression of an "XBP1 gene signature" was associated with worse RFS in patients with triple-negative (TNBC) or estrogen receptor–negative (ESR^-) breast cancers, but not in those with non-TNBC or estrogen receptor–positive (ESR^+) cancers (15, 28). To test the hypothesis that our screening hits also correlated with breast cancer patient survival, we performed survival analyses on an 1,809-patient dataset (26, 28), using a cutoff of the median expression value for each gene. Higher expression of *BCL10*, *GCLM*, and *IGF1R* was significantly associated with worse RFS in patients with TNBC (Fig. 3A; Supplementary Fig. S4A) or ESR^- (Fig. 3B; Supplementary Fig. S4B). Interestingly, higher expression of *GCLM* was also significantly associated with worse RFS in patients with non-TNBC or ESR^+ breast cancer patients (Supplementary Fig. S4A and S4B), suggesting that GCLM is an important mediator of survival in all populations of breast cancer patients.

Next, to validate the role of BCL10, GCLM, and IGF1R in XBP1 activation under ER stress in human breast cancer cells,

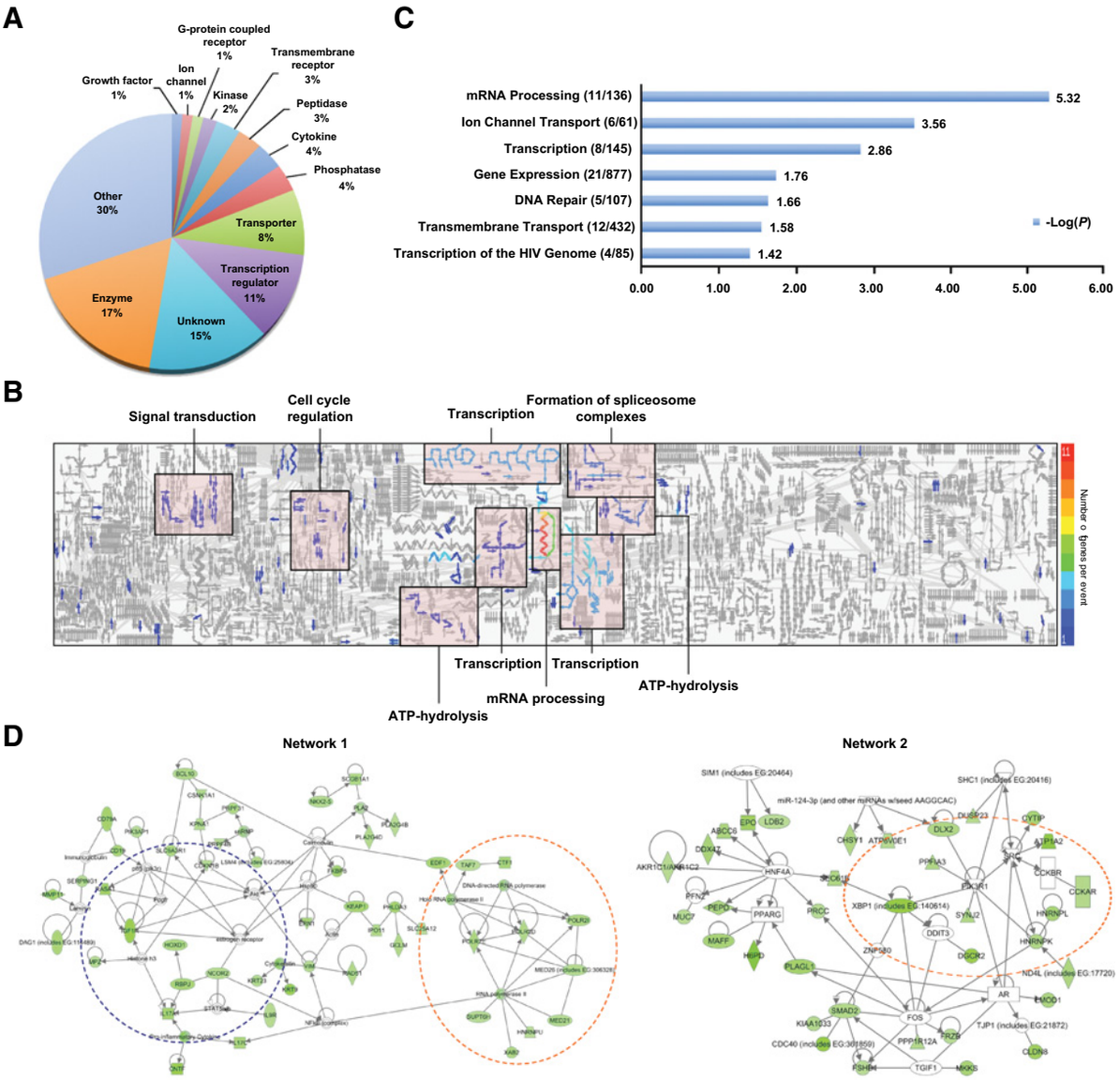

Figure 2.

Functional classification and pathway analysis of siRNA screen results. **A,** Pie graph showing functional classification of candidate genes based on Gene Ontology analyses. **B,** An overview of enriched pathways generated by Reactome Skypainter analysis. The number of identified genes in each signaling event ranging from 1 to 11 was colored from blue to red accordingly. Enriched reaction groups were highlighted in pink box frames. **C,** Negative log [*P* values] of enriched signaling events. Number of identified genes versus total number of genes in each particular event was listed. **D,** Two major signaling networks generated using Ingenuity Pathway Analysis. Screen-identified candidate genes are highlighted in green. Orange dashed circles contain groups of genes involved in mRNA processing; blue dashed circle encompasses a subset of genes related to estrogen receptor signaling.

we deleted expression of *BCL10* or *GCLM* in MCF7 (ESR^+) and MDA-MB-231 (TNBC) cells using a CRISPR/Cas9 approach. Deletion of *BCL10* significantly inhibited bortezomib or thapsigargin-induced XBP1 splicing in both MCF7 and MDA-MB-231 cells (Fig. 3C). Knockout of *GCLM* inhibited bortezomib- or thapsigargin-induced XBP1 splicing in MDA-MB-231 cells, and we further confirmed this result in a second TNBC (MDA-MB-468 cells; Supplementary Fig. S4C). Deletion of *GCLM* in ESR^+ breast cancer cells (MCF7, T47D) yielded uninterpretable results (data not shown). Furthermore, we were not able to delete *IGF1R* in these human breast cancer cell lines by CRISPR/Cas9, likely due to severely compromised cell viability upon loss of IGF1R expression. Nevertheless, we utilized MEFs expressing IGF1R (R^+ cells) and the IGF1R-null MEF cells (R^- cells; ref. 24) and showed that XBP1 activation under ER stress was significantly reduced in R^- cells, compared with R^+ cells (Supplementary Fig. S5A). Furthermore, siRNA knockdown of *IGF1R* expression significantly inhibited bortezomib- or thapsigargin-induced XBP1 splicing in both MCF7 and MDA-MB-231 cells (Fig. 3C).

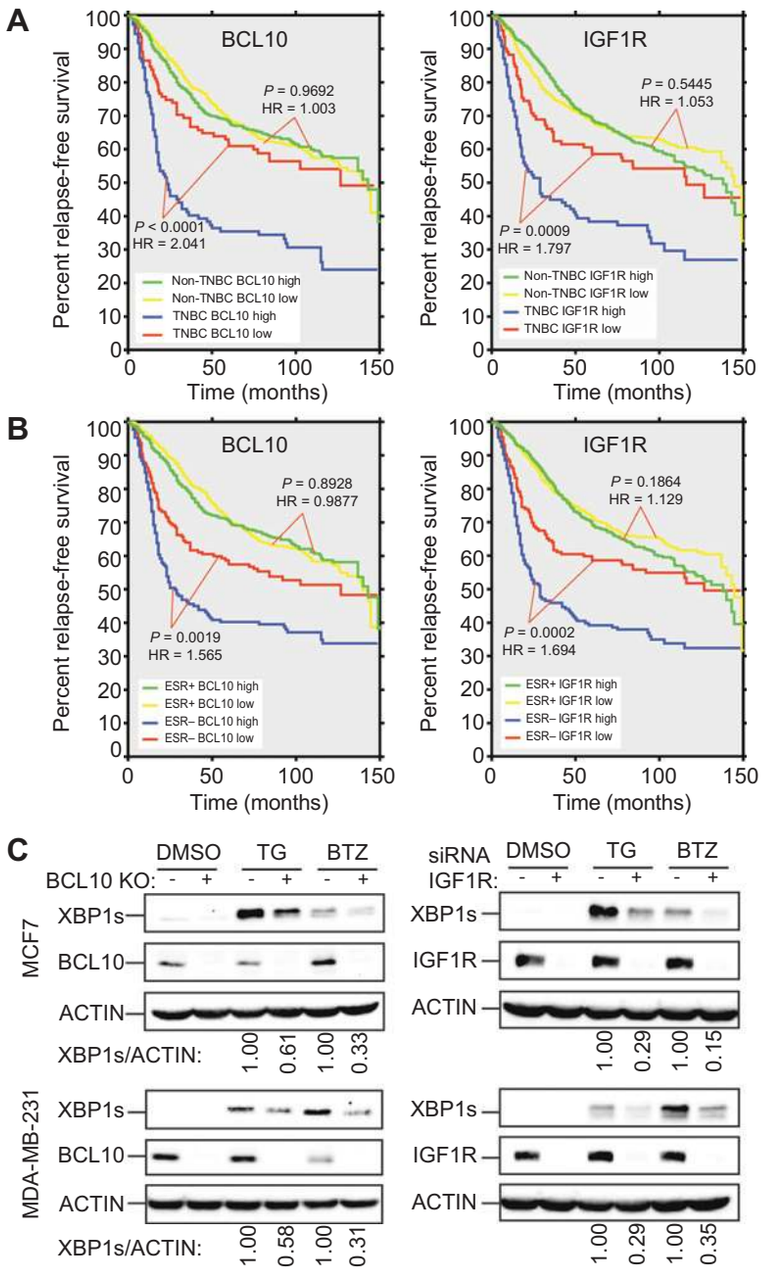

Figure 3.

Validation of the screen hits. **A** and **B,** Kaplan–Meier graphs of RFS for 225 TNBC and 1,415 non-TNBC patients in **A** or 1,286 ESR^+ and 354 ESR^- breast cancer patients in **B** from the same patient cohort, stratified by high and low expression of *BCL10* (left graph) or *IGF1R* (right graph). High BCL10 and IGF1R expression resulted in worse RFS in TNBC and ESR^- patients. The *P* values after Benjamini–Hochberg correction from log-rank (Mantel–Cox) test and the HRs (higher expression compared with lower expression) are shown. **C,** Reduction in ESR stress–induced XBP1s expression after CRISPR/Cas9-mediated knockout of *BCL10* or siRNA-mediated knockdown of *IGF1R*. MCF7 or MDA-MB-231 cells deficient in BCL10 expression or IGF1R expression were treated with thapsigargin (TG, 300 nmol/L) or bortezomib (BTZ, 100 nmol/L) for 14 hours, and Western blotting was performed. Quantification of XBP1s/actin ratio is shown below each blot.

To further demonstrate the correlation between BCL10, GCLM, or IGF1R expression and XBP1 activation, we analyzed a 1,182 breast cancer patient dataset from TCGA. Statistical analysis revealed a significant correlation between the XBP1 gene signature with BCL10, GCLM, or IGF1R expression (Supplementary Fig. S5B). We also evaluated the staining intensity of XBP1s versus IGF1R or GCLM in a tissue microarray made up of 150 cores of human breast cancer specimens. Overall, we found that the expression of XBP1s and IGF1R or GCLM protein was highly correlated (Supplementary Fig. S5C and data not shown). Taken together, these results demonstrate the feasibility of identifying important genes that regulate IRE1α–XBP1 signaling through genome-wide siRNA screen. These studies also provide strong evidence to support the clinical significance of IRE1α–XBP1 signaling in the prognosis of breast cancers.

Significance

The IRE1α–XBP1 pathway plays an indispensable role in tumor growth, metastatic progression, and chemoresistance (7, 8, 15). XBP1 has been extensively characterized as a mediator of cell survival in many tumor types. Expression and activation of XBP1 has been correlated with poor clinical outcome in breast cancer (14, 15) and angiogenesis in pancreatic cancer (16). Here, we performed a genome-wide, loss-of-function, luciferase reporter–based siRNA screen, through which we identified and characterized

a group of 162 novel genes involved in the regulation of the IRE1α–XBP1 signaling branch of the UPR. To ensure the accuracy of our screening hits, we confirmed that 88% of our positive hits were indeed involved in bortezomib-induced XBP1 activation. The enriched molecular pathways from these genes suggest that a variety of biological processes and signaling networks may influence XBP1 splicing, thus providing important biological insights into UPR regulation and suggesting new therapeutic strategies for diseases in which the UPR is deregulated. Furthermore, our study highlights the value of combining genome-wide loss-of-function screen, bioinformatics analysis, and postscreen validation to comprehensively elucidate the global regulation of a complex signaling pathway.

Disclosure of Potential Conflicts of Interest

No potential conflicts of interest were disclosed.

Authors' Contributions

Conception and design: Z. Yang, J. Zhang, D. Jiang, N.C. Denko, A.J. Giaccia, Q.-T. Le, A.C. Koong
Development of methodology: Z. Yang, J. Zhang, D. Jiang, P. Khatri, D.E. Solow-Cordero, A.C. Koong
Acquisition of data (provided animals, acquired and managed patients, provided facilities, etc.): Z. Yang, J. Zhang, D. Jiang, D.E. Solow-Cordero, D.A.S. Toesca, A.C. Koong
Analysis and interpretation of data (e.g., statistical analysis, biostatistics, computational analysis): Z. Yang, J. Zhang, D. Jiang, P. Khatri, D.E. Solow-Cordero, D.A.S. Toesca, N.C. Denko, Q.-T. Le, A.C. Koong
Writing, review, and/or revision of the manuscript: Z. Yang, J. Zhang, D. Jiang, P. Khatri, D.A.S. Toesca, C. Koumenis, N.C. Denko, Q.-T. Le, A.C. Koong
Administrative, technical, or material support (i.e., reporting or organizing data, constructing databases): Z. Yang, D. Jiang, D.E. Solow-Cordero, C. Koumenis, A.C. Koong
Study supervision: Z. Yang, C. Koumenis, A.C. Koong

Acknowledgments

The authors acknowledge support from NIH R01 CA161585-01A1 (to A.C. Koong and Q.T. Le,), NIH PPG grant P01-CA67166 (to A.C. Koong, Q.T. Le, and A.J. Giaccia), My Blue Dots Foundation (to A.C. Koong), the National Library of Medicine T15 LM007033 (to P. Khatri), and the University of Pennsylvania Pharmacological Targeting of the Unfolded Protein Response as an Antitumor Strategy Grant (to J. Zhang, A.C. Koong, and C. Koumenis).

The authors thank Dr. Andrea Morrione and Dr. Renato Baserga (Thomas Jefferson University) for kindly providing us the R^- and R^+ MEFs. We thank Jason Wu at Stanford High-throughput Facility, Katie Planey in the Department of Pediatrics at Stanford University, Alice Banh, Hongbin Cao, Peiwen Kuo, and Tori Xiao in Dr. Quynh-Thu Le's laboratory, and members of Dr. Amato Giaccia's laboratory for general discussion and technical assistance.

Received June 15, 2017; revised November 2, 2017; accepted February 5, 2018; published first February 9, 2018.

References

1. Walter P, Ron D. The unfolded protein response: from stress pathway to homeostatic regulation. Science 2011;334:1081–6.
2. Xiang C, Wang Y, Zhang H, Han F. The role of endoplasmic reticulum stress in neurodegenerative disease. Apoptosis 2017;22:1–26.
3. Korennykh AV, Egea PF, Korostelev AA, Finer-Moore J, Zhang C, Shokat KM, et al. The unfolded protein response signals through high-order assembly of Ire1. Nature 2009;457:687–93.
4. Lee KP, Dey M, Neculai D, Cao C, Dever TE, Sicheri F. Structure of the dual enzyme Ire1 reveals the basis for catalysis and regulation in nonconventional RNA splicing. Cell 2008;132:89–100.
5. Hetz C, Chevet E, Harding HP. Targeting the unfolded protein response in disease. Nat Rev Drug Discov 2013;12:703–19.
6. Ozcan U, Cao Q, Yilmaz E, Lee AH, Iwakoshi NN, Ozdelen E, et al. Endoplasmic reticulum stress links obesity, insulin action, and type 2 diabetes. Science 2004;306:457–61.
7. Jiang D, Niwa M, Koong AC. Targeting the IRE1α-XBP1 branch of the unfolded protein response in human diseases. Semin Cancer Biol 2015;33:48–56.
8. Cubillos-Ruiz JR, Bettigole SE, Glimcher LH. Tumorigenic and immunosuppressive effects of endoplasmic reticulum stress in cancer. Cell 2017;168:692–706.
9. Romero-Ramirez L, Cao H, Nelson D, Hammond E, Lee AH, Yoshida H, et al. XBP1 is essential for survival under hypoxic conditions and is required for tumor growth. Cancer Res 2004;64:5943–7.
10. Carrasco DR, Sukhdeo K, Protopopova M, Sinha R, Enos M, Carrasco DE, et al. The differentiation and stress response factor XBP-1 drives multiple myeloma pathogenesis. Cancer Cell 2007;11:349–60.
11. Nakamura M, Gotoh T, Okuno Y, Tatetsu H, Sonoki T, Uneda S, et al. Activation of the endoplasmic reticulum stress pathway is associated with survival of myeloma cells. Leuk Lymphoma 2006;47:531–9.
12. Iwakoshi NN, Lee AH, Vallabhajosyula P, Otipoby KL, Rajewsky K, Glimcher LH. Plasma cell differentiation and the unfolded protein response intersect at the transcription factor XBP-1. Nat Immunol 2003;4:321–9.
13. Munshi NC, Hideshima T, Carrasco D, Shammas M, Auclair D, Davies F, et al. Identification of genes modulated in multiple myeloma using genetically identical twin samples. Blood 2004;103:1799–806.
14. Davies MP, Barraclough DL, Stewart C, Joyce KA, Eccles RM, Barraclough R, et al. Expression and splicing of the unfolded protein response gene XBP-1 are significantly associated with clinical outcome of endocrine-treated breast cancer. Int J Cancer 2008;123:85–8.
15. Chen X, Iliopoulos D, Zhang Q, Tang Q, Greenblatt MB, Hatziapostolou M, et al. XBP1 promotes triple-negative breast cancer by controlling the HIF1alpha pathway. Nature 2014;508:103–7.
16. Romero-Ramirez L, Cao H, Regalado MP, Kambham N, Siemann D, Kim JJ, et al. X box-binding protein 1 regulates angiogenesis in human pancreatic adenocarcinomas. Translat Oncol 2009;2:31–8.
17. Tang CH, Ranatunga S, Kriss CL, Cubitt CL, Tao J, Pinilla-Ibarz JA, et al. Inhibition of ER stress-associated IRE-1/XBP-1 pathway reduces leukemic cell survival. J Clin Invest 2014;124:2585–98.
18. Chen L, Li Q, She T, Li H, Yue Y, Gao S, et al. IRE1α-XBP1 signaling pathway, a potential therapeutic target in multiple myeloma. Leuk Res 2016;49:7–12.
19. Papandreou I, Denko NC, Olson M, Van Melckebeke H, Lust S, Tam A, et al. Identification of an Ire1alpha endonuclease specific inhibitor with cytotoxic activity against human multiple myeloma. Blood 2011;117:1311–4.
20. Mimura N, Fulciniti M, Gorgun G, Tai YT, Cirstea D, Santo L, et al. Blockade of XBP1 splicing by inhibition of IRE1alpha is a promising therapeutic option in multiple myeloma. Blood 2012;119:5772–81.
21. Park SW, Zhou Y, Lee J, Lu A, Sun C, Chung J, et al. The regulatory subunits of PI3K, p85alpha and p85beta, interact with XBP-1 and increase its nuclear translocation. Nat Med 2010;16:429–37.
22. Koumenis C, Bi M, Ye J, Feldman D, Koong AC. Hypoxia and the unfolded protein response. Methods Enzymol 2007;435:275–93.
23. Fels DR, Ye J, Segan AT, Kridel SJ, Spiotto M, Olson M, et al. Preferential cytotoxicity of bortezomib toward hypoxic tumor cells via overactivation of endoplasmic reticulum stress pathways. Cancer Res 2008;68:9323–30.
24. Sell C, Rubini M, Rubin R, Liu JP, Efstratiadis A, Baserga R. Simian virus 40 large tumor antigen is unable to transform mouse embryonic fibroblasts lacking type 1 insulin-like growth factor receptor. Proc Natl Acad Sci U S A 1993;90:11217–21.
25. Sanjana NE, Shalem O, Zhang F. Improved vectors and genome-wide libraries for CRISPR screening. Nat Methods 2014;11:783–4.
26. Gyorffy B, Lanczky A, Eklund AC, Denkert C, Budczies J, Li Q, et al. An online survival analysis tool to rapidly assess the effect of 22,277 genes on breast cancer prognosis using microarray data of 1,809 patients. Breast Cancer Res Treat 2010;123:725–31.
27. Karn T, Metzler D, Ruckhäberle E, Hanker L, Gätje R, Solbach C, et al. Data-driven derivation of cutoffs from a pool of 3,030 Affymetrix arrays to

stratify distinct clinical types of breast cancer. Breast Cancer Res Treat 2010;120:567–79.
28. Jiang D, Turner B, Song J, Li R, Diehn M, Le QT, et al. Comprehensive analysis of the unfolded protein response in breast cancer subtypes. JCO Precision Oncology 2017 July 26. Available from: http://ascopubs.org/doi/full/10.1200/PO.16.00073.
29. Spiotto MT, Banh A, Papandreou I, Cao H, Galvez MG, Gurtner GC, et al. Imaging the unfolded protein response in primary tumors reveals microenvironments with metabolic variations that predict tumor growth. Cancer Res 2010;70:78–88.
30. Landowski TH, Megli CJ, Nullmeyer KD, Lynch RM, Dorr RT. Mitochondrial-mediated disregulation of Ca^{2+} is a critical determinant of Velcade (PS-341/bortezomib) cytotoxicity in myeloma cell lines. Cancer Res 2005;65:3828–36.
31. Obeng EA, Carlson LM, Gutman DM, Harrington WJ Jr., Lee KP, Boise LH. Proteasome inhibitors induce a terminal unfolded protein response in multiple myeloma cells. Blood 2006;107:4907–16.
32. Harris IS, Treloar AE, Inoue S, Sasaki M, Gorrini C, Lee KC, et al. Glutathione and thioredoxin antioxidant pathways synergize to drive cancer initiation and progression. Cancer Cell 2015;27:211–22.
33. Keeton EK, Brown M. Cell cycle progression stimulated by tamoxifen-bound estrogen receptor-alpha and promoter-specific effects in breast cancer cells deficient in N-CoR and SMRT. Mol Endocrinol 2005;19:1543–54.
34. Alkarain A, Jordan R, Slingerland J. p27 deregulation in breast cancer: prognostic significance and implications for therapy. J Mammary Gland Biol Neoplasia 2004;9:67–80.
35. Wang L, Jiang Y, Zhang Y, Wang Y, Huang S, Wang Z, et al. Association analysis of IL-17A and IL-17F polymorphisms in Chinese Han women with breast cancer. PLoS One 2012;7:e34400.
36. Cancer Genome Atlas Network. Comprehensive molecular portraits of human breast tumours. Nature 2012;490:61–70.
37. Pan D, Zhu Y, Zhou Z, Wang T, You H, Jiang C, et al. The CBM complex underwrites NF-κB activation to promote HER2-associated tumor malignancy. Mol Cancer Res 2016;14:93–102.
38. Wu T, Zhao F, Gao B, Tan C, Yagishita N, Nakajima T, et al. Hrd1 suppresses Nrf2-mediated cellular protection during liver cirrhosis. Genes Dev 2014;28:708–22.
39. Dong L, Jiang CC, Thorne RF, Croft A, Yang F, Liu H, et al. Ets-1 mediates upregulation of Mcl-1 downstream of XBP-1 in human melanoma cells upon ER stress. Oncogene 2011;30:3716–26.
40. Endo H, Murata K, Mukai M, Ishikawa O, Inoue M. Activation of insulin-like growth factor signaling induces apoptotic cell death under prolonged hypoxia by enhancing endoplasmic reticulum stress response. Cancer Res 2007;67:8095–103.
41. Wheeler MC, Gekakis N. Defective ER associated degradation of a model luminal substrate in yeast carrying a mutation in the 4th ER luminal loop of Sec61p. Biochem Biophys Res Commun 2012;427:768–73.
42. Novosyadlyy R, Kurshan N, Lann D, Vijayakumar A, Yakar S, LeRoith D. Insulin-like growth factor-I protects cells from ER stress-induced apoptosis via enhancement of the adaptive capacity of endoplasmic reticulum. Cell Death Differ 2008;15:1304–17.